Alectinib enhances response to RBM39 degradation via SRPK1 inhibition

Authors: Yurui Ma[1], Evon Poon[2], Chenchen Jin[1], Barbara Martins da Costa[2], Yuewei Xu[1,3], Sadiya Quazi[1], Nikolaos Zourdoumis[1], Chiharu Wickremesinghe[1], Louis Chesler[2], Hector C Keun[1]*, Anke Nijhuis[1]*¥

Affiliations:

[1]Department of Surgery & Cancer, Imperial College London; London, UK.

[2]Division of Clinical Studies, The Institute of Cancer Research, London, UK

[3]Wisdom Lake Academy of Pharmacy, Xi'an Jiaotong-Liverpool University, Suzhou 215123, China (current affiliation)

***Co-corresponding author**

¥**Lead contact:** Dr Anke Nijhuis

Address: Division of Cancer, Imperial College London, London, UK, W12 0NN.

Email: a.nijhuis@imperial.ac.uk **Phone**: +44 (0) 20 7594 3161

One Sentence Summary: Dual RNA splicing interference by indisulam and alectinib enhances sensitivity in MYCN-driven malignancies such as high-risk neuroblastoma, increasing DNA damage and R-loop accumulation.

Abstract: RNA splicing is a critical process in gene expression regulation and RNA splicing factors are increased in expression in many cancers. We have previously demonstrated that the molecular glue indisulam degrades RNA splicing factor RBM39 producing aberrant splicing

transcripts that is very effective in high-risk neuroblastoma and can potentiate the sensitivity to DNA damaging agents in ovarian high-grade serous carcinoma. RNA splicing inhibitors have the ability to generate vulnerabilities that can be exploited for combinatorial therapeutic strategies. In this study, we employed combination drug screens to identify potential synergistic drug-drug interactions between indisulam and other FDA approved clinical compounds. We demonstrate that alectinib, a clinically approved ALK inhibitor, has strong potency against serine/arginine protein kinase 1 (SRPK1), a key modulator of RNA splicing. Combined treatment with alectinib and indisulam leads to synergistic cell growth inhibition, increased cell apoptosis and cell cycle arrest in multiple cancer cell lines including high-risk neuroblastoma. Co-treatment exacerbated RNA splicing defects in genes involved in DNA damage response and R-loop resolution, leading to R-loop accumulation and increased DNA damage. In the Th-MYCN/ALK^{F1174L} neuroblastoma mouse model, combination therapy induced complete tumour regression and significantly improved survival rates compared with monotherapies.

Thus, the combination of indisulam and alectinib is a promising approach to treat aggressive malignancies such MYCN-driven high-risk neuroblastoma, exploiting the hitherto untapped pharmacology of alectinib as a clinical RNA splicing inhibitor. Our work demonstrates the concept that co-targeting of functionally interdependent RNA splicing factors is a strategy that can yield new and highly synergistic anti-cancer combination therapies effective against otherwise hard-to-treat cancers.

Main Text:

INTRODUCTION

43 The splicing of precursor messenger RNAs (pre-mRNAs) is a critical regulatory step in gene
44 expression, during which non-coding introns are excised to produce functional mRNA(*1*). This
45 process is tightly controlled by splicing factors, governing the recognition and selection of splice
46 sites, thereby generating mRNAs with varying exon combinations and consequently diverse
47 protein isoforms(*1*). Dysregulated alternative splicing can promote tumorigenesis and
48 chemoresistance. Aryl sulfonamides such as indisulam have emerged as promising anticancer
49 agents by targeting a pre-mRNA splicing factor RBM39 (RNA binding motif 39)(*2, 3*). These
50 molecular glues facilitate the association of RBM39 with the CUL4-DCAF15 ubiquitin ligase,
51 resulting in RBM39 polyubiquitination and subsequent proteasomal degradation(*2, 4*).
52 Suppressing RBM39 efficiently inhibits tumour growth and advancement through modulating the
53 transcription of various genes associated with tumorigenesis (reviewed in (*3*)).
54 One cancer type particularly vulnerable to splicing perturbation is neuroblastoma (*5-8*), a common
55 and aggressive extracranial solid tumour in young children, which represents a significant
56 contributor to mortality in children with cancer(*9*). High-risk neuroblastoma, comprising
57 approximately 15% of all neuroblastoma cases, represents a distinct subtype characterized by
58 aggressive tumour behaviour and an unfavourable prognosis(*10*). One pivotal factor contributing
59 to the progression of high-risk neuroblastoma is the amplification of the MYC family transcription
60 factor, MYCN, which can block the differentiation of neural progenitors, the key event in
61 neuroblastoma initiation(*11*), and plays a crucial role in facilitating the transcriptional repression
62 of tumour suppressor genes(*9, 10*). Furthermore, oncogenic gain-of-function mutations in the *ALK*
63 (Anaplastic Lymphoma Kinase) occur in 10–15% of primary tumours, making ALK the most
64 common single-gene alteration in high-risk neuroblastoma for which targeted clinical therapies
65 have been developed(*9, 12*) Alectinib, an FDA-approved ATP-competitive ALK tyrosine kinase

66 inhibitor (TKI),was initially developed for non-small-cell lung cancer and has shown considerable
67 promise in addressing neuroblastoma in extensive preclinical studies(*13-15*). However, tumour
68 heterogeneity and resistance to treatment with ALK inhibitors (and molecularly-targeted drugs in
69 general) limits their use as single agents (*16*). Thus, novel strategies, particularly combination
70 therapies, remain important as a means to reduce the toxicity of any single drug and overcome
71 treatment resistance more efficiently. This approach is particularly advantageous in childhood
72 cancer, where long-term toxicity is a major lifelong issue (*17*).
73
74 Our previous study(*6*) and others(*8*) have recognized the exquisite sensitivity of high-risk
75 neuroblastoma to indisulam, with complete responses observed in multiple xenografts, patient-
76 derived xenografts (PDX) and transgenic mouse models. Notably, our study reported that cells
77 with MYCN amplification displayed heightened sensitivity to aryl sulfonamides in comparison to
78 those without MYCN amplification. This could be attributed to the increased reliance of
79 neuroblastoma cells on RNA processing due to elevated N-Myc/c-Myc activity, rendering them
80 more susceptible to RNA splicing interference (*18*). Through the induction of splicing errors in
81 genes within key oncogenic pathways, indisulam can render cancer cells susceptible to additional
82 disruptions caused by other anticancer drugs. For example, we have previously shown that several
83 key DNA damage repair (DDR) genes are mis-spliced after RBM39 depletion (such as *BRCA1*,
84 *RAD51D* and *ATM*), and therefore that indisulam treatment can increase sensitivity to PARP
85 inhibitors in ovarian high-grade serous carcinoma (*19*).
86
87 In this study, we aimed to identify additional vulnerabilities through drug-drug library screens
88 combining indisulam with FDA approved anti-cancer agents. Through this, we demonstrate a

89 novel synergistic interaction between indisulam and ALK-inhibitor alectinib, likely due to activity
90 against a recently discovered secondary target of alectinib, RNA Serine-Arginine Protein Kinase
91 1 (SRPK1) (*20*). SRPK1 promotes the nuclear translocation and activation of a family of SR
92 splicing factors (SRSFs). The combination of indisulam and alectinib simultaneously depletes
93 RBM39 and inhibits SRPK1-mediated SRSF phosphorylation, resulting in exacerbated RNA
94 splicing defects. The subsequent failure to resolve accumulated DNA damage and R loops results
95 in cell cycle arrest, cell growth inhibition and apoptosis of neuroblastoma cells *in-vitro* and tumour
96 regression *in vivo*. Our study provides important proof-of-concept evidence for the co-targeting of
97 splicing factors as a viable strategy to treat aggressive malignancies such as MYCN-driven high-
98 risk neuroblastoma.

99

100 **RESULTS**

101 **Combination drug screens revealed synergy between indisulam and alectinib.**

102 We previously demonstrated that indisulam-mediated RBM39 degradation causes wide-spread
103 RNA splicing defects, and an enrichment in aberrant expression of proteins that mediate DNA
104 damage repair and cell cycle regulation, across various cancer types(*6, 19*). This led us to speculate
105 that indisulam is likely to generate drug-induced-vulnerabilities that potentiate the efficacy of
106 existing, clinically approved anti-cancer compounds, such as PARP inhibitors(*19*). RBM39
107 degraders, such as indisulam and E7820, have been trialed in 47 clinical studies(*3*), highlighting
108 potential therapeutic combinations ready for clinical evaluation.

109

110 To explore this concept, we conducted two drug-library screens combining indisulam with 147
111 FDA-approved anticancer drugs (NCI plate number #4891, #4892) in an indisulam-sensitive cell

line (HCT116, colorectal cancer) and an indisulam-resistant line (KURAMOCHI, ovarian cancer). Anticancer compounds were tested at 5 doses ranging from 16nM to 10μM based on the average GI50 value, and combined with DMSO or indisulam at a fixed dose (GI30=50nM, for HCT116, 10μM for KURAMOCHI) (**Fig. 1A, Fig. S1A**). Bliss scores(*21*) were calculated to identify synergistic interactions with indisulam. Depletion of RBM39 by indisulam is dependent on DCAF15 expression, thus we generated CRISPR-Cas9 knockouts of *DCAF15* to identify RBM39-specific drug-drug interactions (HCT116 *DCAF15* wild-type (*DCAF15*^{WT}) clone #1 and #2 and *DCAF15* knock-out clones (*DCAF15*^{KO}) clone #1 and #2). Drugs with Bliss score>0 in both HCT116-*DCAF15*^{WT} clones were selected as hits which were further validated in triplicate experiments with selected doses in both HCT116-*DCAF15*^{WT} and *DCAF15*^{KO} clones #1 and #2 and ranked by mean Bliss scores of both cell lines. Most of the synergistic drug-drug interactions were rescued in HCT116-*DCAF15*^{KO} cells suggesting that the synergy is dependent on *DCAF15* and RBM39 degradation (**Fig. 1B left**). In KURAMOCHI, the top 20 hits were ranked by mean Bliss scores across all doses (**Fig. 1B right**). The clinical ALK inhibitor alectinib demonstrated strong synergy in both HCT116 (top hit) and KURAMOCHI (second hit) and was therefore selected for further validation using a wider range of drug concentrations. Strong synergistic growth inhibition was observed across a range of doses of indisulam and alectinib in HCT116 (**Fig. 1C**) and KURAMOCHI (**Fig. 1D**), and the synergy was abrogated in HCT116-*DCAF15*^{KO} cells.

These data confirm that the combination of alectinib with RBM39 degraders exert strong synergistic inhibition of cell growth in HCT116 and KURAMOCHI cells and this highlights an opportunity for the development of a novel combination therapy across genomically diverse cancer types.

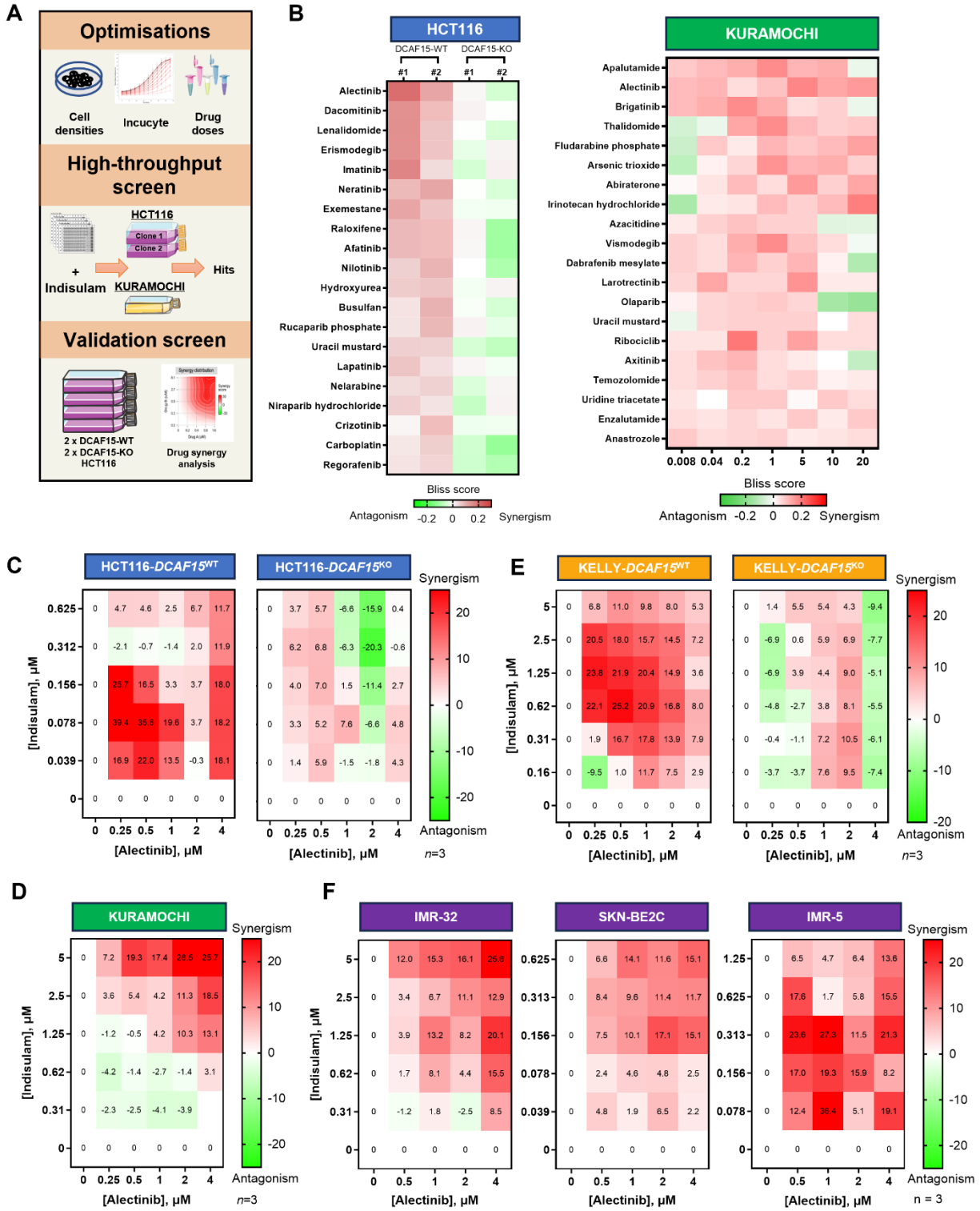
A
Optimisations
Cell densities
Incucyte
Drug doses
High-throughput screen
HCT116
Clone 1
Clone 2
+
Indisulam
KURAMOCHI
Hits
Validation screen
2 x DCAF15-WT
2 x DCAF15-KO
HCT116
Drug synergy analysis
B
HCT116
DCAF15-WT
DCAF15-KO
#1
#2
#1
#2
Alectinib
Dacomitinib
Lenalidomide
Erismodegib
Imatinib
Neratinib
Exemestane
Raloxifene
Afatinib
Nilotinib
Hydroxyurea
Busulfan
Rucaparib phosphate
Uracil mustard
Lapatinib
Nelarabine
Niraparib hydrochloride
Crizotinib
Carboplatin
Regorafenib
Bliss score
Antagonism -0.2 0 0.2 Synergism
KURAMOCHI
Apalutamide
Alectinib
Brigatinib
Thalidomide
Fludarabine phosphate
Arsenic trioxide
Abiraterone
Irinotecan hydrochloride
Azacitidine
Vismodegib
Dabrafenib mesylate
Larotrectinib
Olaparib
Uracil mustard
Ribociclib
Axitinib
Temozolomide
Uridine triacetate
Enzalutamide
Anastrozole
0.008 0.04 0.2 1 5 10 20
Bliss score
Antagonism -0.2 0 0.2 Synergism
C
HCT116-DCAF15WT
HCT116-DCAF15KO
[Indisulam], µM
[Alectinib], µM
Synergism
Antagonism
n=3
E
KELLY-DCAF15WT
KELLY-DCAF15KO
[Indisulam], µM
[Alectinib], µM
Synergism
Antagonism
n=3
D
KURAMOCHI
[Indisulam], µM
[Alectinib], µM
Synergism
Antagonism
n=3
F
IMR-32
SKN-BE2C
IMR-5
[Indisulam], µM
[Alectinib], µM
Synergism
Antagonism
n = 3

135

136

137 **Figure 1. Combination drug screens revealed a synergistic growth inhibition of indisulam and alectinib.** (**A**)
138 Workflow of combination drug screens in HCT116 and KURAMOCHI using indisulam and 147 FDA-approved
139 anticancer compounds. (**B**) Top 20 hits from drug screens in HCT116 (left) and KURAMOCHI (right). Two HCT116-
140 *DCAF15*^{WT} or HCT116-*DCAF15*^{KO} cell lines treated with selected hits with or without indisulam. Bliss scores were
141 calculated based on cell growth measured by SRB assay. Hits are ranked by mean bliss scores of both *DCAF15*^{WT}
142 clones. Bliss score > 0 (red) indicates synergism, n=3 replicates. KURAMOCHI cells were treated with indicated
143 doses of drugs, with or without indisulam; Top 20 hits are ranked by mean bliss score. Bliss score > 0 (red) indicates
144 synergism, n=3 replicates. (**C-F**) Cell lines used for synergy screen (C, D) and indicated HRNB cell lines (E, F) were
145 treated with alectinib combining indisulam for 72 hours and analysed for cell growth by SRB. Synergy scores were
146 calculated by Synergyfinder (https://synergyfinder.fimm.fi/) using the Loewe method.

147

148 **Indisulam and alectinib exhibit synergistic anticancer efficacy in high-risk neuroblastoma**

149 Considering the potency demonstrated by both indisulam and alectinib as monotherapies in high-
150 risk neuroblastoma(*6, 14*), we further investigated the combination of indisulam and alectinib in
151 four high-risk neuroblastoma cell lines (KELLY, IMR32, SKNBE2C, IMR5) (**Fig. 1E-F**). We
152 demonstrate that combining alectinib with indisulam significantly inhibits cell proliferation
153 compared to monotherapies and display great synergy across a wide-range doses of both
154 compounds on neuroblastoma cell lines, but only additive or antagonistic effects were found in
155 KELLY-*DCAF15*^{KO} cell line confirming the necessity of RBM39 degradation for this
156 pharmacological interaction (**Fig. 1E right**). Similar synergy profiles were observed between
157 alectinib and E7820, a second aryl sulfonamide RBM39 degrader (*2*)(**Fig. S1B-C**).

158

159 In addition, alectinib treatment alone did not induce cell apoptosis, but significantly increased the
160 percentage of apoptotic cells when combined with indisulam in KELLY and IMR32 (**Fig. 2A-B,**
161 **Fig. S2D**). Correspondingly, a significant increase of cleaved caspase 3 was detected in the

162 combination treatment group in KELLY cells (**Fig. 2C**). To evaluate cell cycle progression, we
163 used flow cytometry analysis and detected a notable accumulation of cells in the G2/M phases
164 following 48-hour treatment of indisulam which is consistent with a previous study(*8*). Co-
165 treatment with indisulam and alectinib increased the percentage of cells in the G1-phase, implying
166 enhanced cell cycle arrest in both G2/M and G1 phase, with a substantial decrease in the percentage
167 of cells in S-phase (**Fig. 2D-E**). These data confirm that indisulam and alectinib act synergistically
168 to suppress the proliferation of neuroblastoma cells, disrupt cell cycle and induce cell apoptosis.
169
170
171

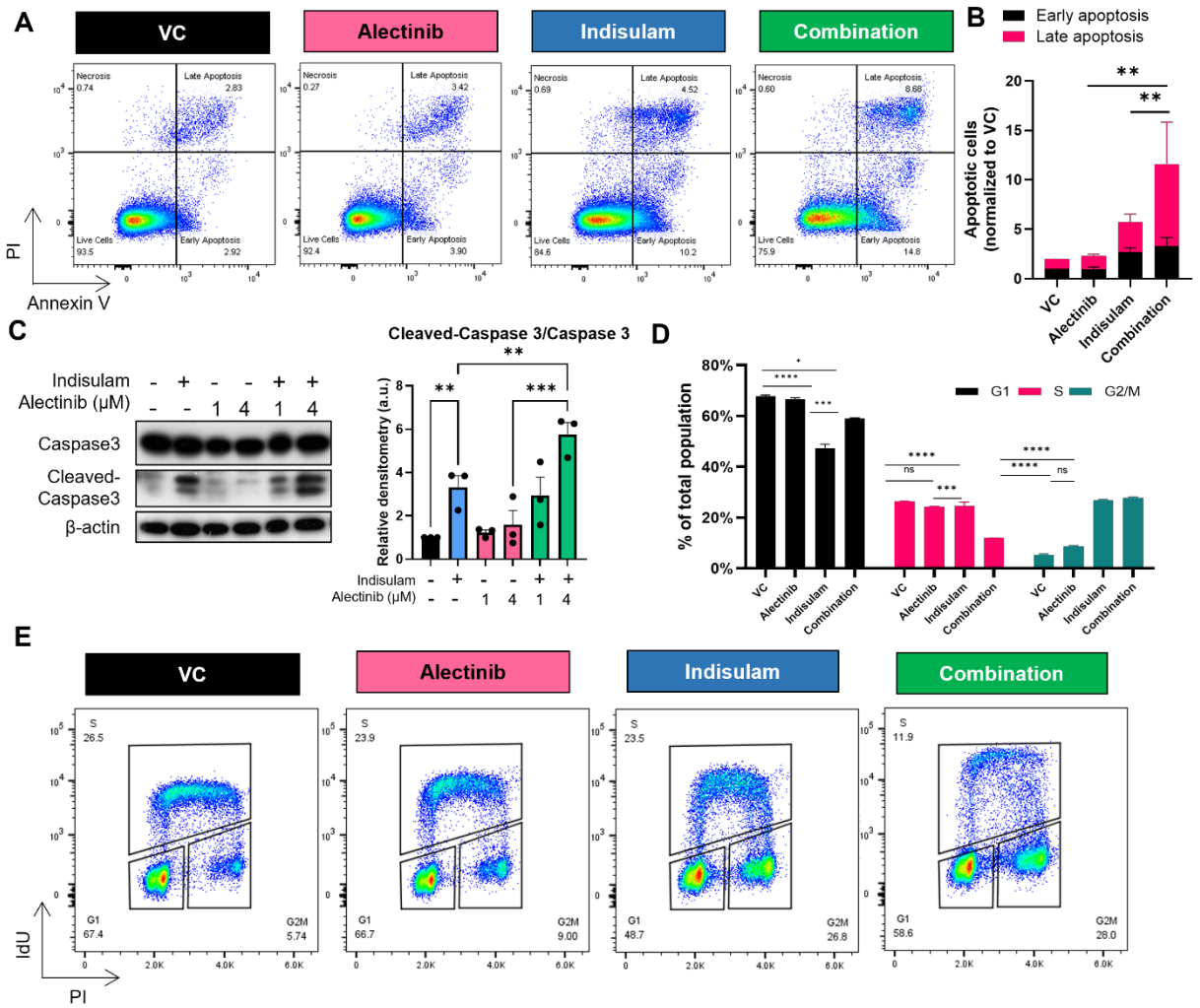

Figure 2. Indisulam and alectinib induce apoptosis and cell cycle disruption in high-risk neuroblastoma. (**A-B**) Apoptosis analysis via flow cytometry in KELLY cells following exposure to 1.25μM indisulam, 4μM alectinib, or their combination for 48 hours. Cells were labelled by Annexin V and propidium iodide (PI). The significance of difference of total apoptotic cells was calculated by one-way ANOVA. (**C**) Western blot of KELLY cells treated with indicated doses of indisulam and alectinib for 48 hours. (n=3 independent experiments) significance of difference was calculated by one-way ANOVA. (**D-E**) Profiling of cell cycle distribution in KELLY cells was performed using flow cytometry after a 48-hour treatment with indisulam, Alectinib, or the combination. Cellular DNA content was labelled with PI, while replicating cells were labelled with nucleotide analogues 5-Iodo-2-deoxyuridine (IdU). Quantitative analysis of cell cycle distribution (n=3 independent experiments). Two-way ANOVA were employed to determine the statistical significance among the groups. n.s. not significant, * $p < 0.05$, ** $p<0.01$, *** $p < 0.001$, **** $p < 0.0001$.

183 **ALK inhibition by alectinib is not required for synergistic interaction with indisulam.**

184 According to data from the Human Protein Atlas (proteinatlas.org) (*22*) ALK and RET, both
185 primary targets of alectinib, are expressed in NB cells but not in HCT116 and KURAMOCHI (**Fig.**
186 **3A, Table S1**) in which synergy was initially discovered. Western blotting confirmed an absence
187 of ALK expression in these cells (**Fig. 3B**). To further test whether the synergy is driven by ALK
188 inhibition, we transfected KELLY, HCT116, and KURAMOCHI cells with an siRNA targeting
189 ALK (siALK) prior to indisulam dosing (**Fig. 3B**). We found no significant difference in cell
190 growth inhibition between siALK and non-targeting control (siNTC) transfected cells (**Fig. 3C**),
191 indicating that ALK inhibition alone does not increase sensitivity to indisulam. We also tested a
192 second ALK inhibitor with a distinct chemical scaffold and binding site, lorlatinib, and found that
193 this compound did not enhance sensitivity to indisulam, except in KELLY cells, which express a
194 mutant, oncogenic form of ALK (ALK^{F1174L}) (**Fig. 3D and Fig. S2A**). However, in cell lines with
195 wild type ALK (IMR32) or lacking ALK expression (HCT116 and KURAMOCHI) there was no
196 sensitization (**Fig. 3D**), consistent with other studies (*23*), indicating that the efficacy of lorlatinib
197 is specific to ALK mutated neuroblastoma. Further experimental validation is needed to clarify the
198 interaction between inhibition of mutant ALK-driven tumours and RBM39 depletion by indisulam.
199 Nonetheless, these findings suggest that ALK inhibition is not a significant contributor to the
200 synergy we observe between alectinib and the RBM39 degraders indisulam and E7820. This
201 suggests that synergy with RBM39 degradation relates primarily to inhibition of a secondary target
202 of alectinib.

203

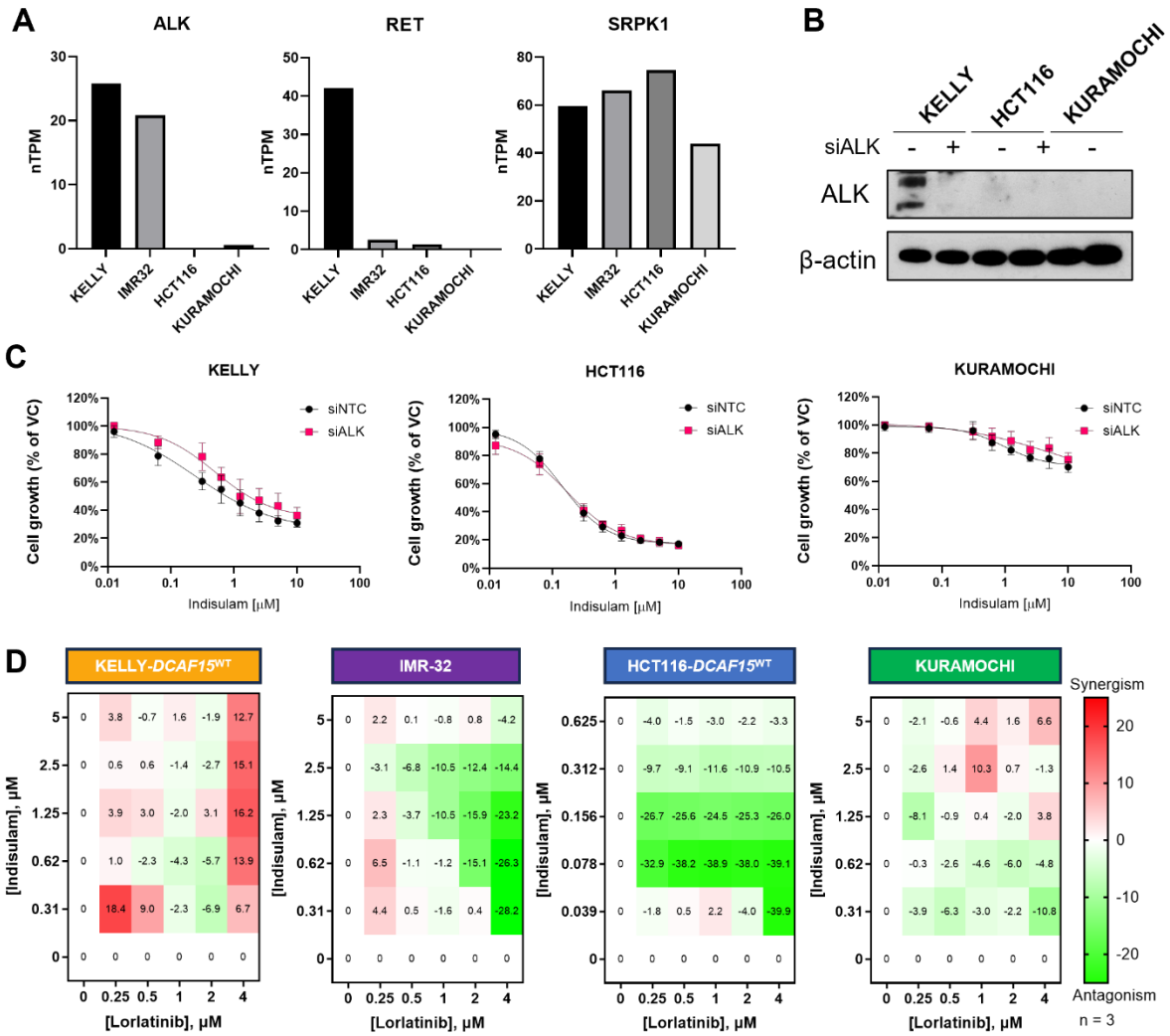

Figure 3. ALK inhibition by alectinib is not an essential determinant of indisulam synergy. (**A**) RNA expression data as normalized transcript per million (nTPM) values of cancer cell lines were obtained from proteinatlas.org. (**B**) Western blot confirming the knock-down of ALK gene expression in cells post transfection with siNTC or siALK. (**C**) Indicated cell lines were transfected with siALK or siNTC for 16 hours, followed by exposure to indisulam for 72 hours. Cell growth was measured by SRB assay. (**D**) Indicated cell lines were treated with lorlatinib and indisulam concentration matrix for 72 hours. Loewe synergy scores are plotted. n=3 replicates.

214 **Alectinib exerts potent inhibition of SRPK1.**

215 Comprehensive kinase inhibitor screens indicate that alectinib inhibits an array of additional
216 kinases other than ALK (*20*). The observation that alectinib is a potent inhibition of Serine/arginine
217 (SR) Protein Kinase 1/2 (SRPK1/2) (*20, 24*) is particularly relevant to our research of aberrant
218 RNA splicing. Both SRPK1 and 2 play a central role in regulation of alternative splicing via
219 phosphorylation and activation and nuclear translocation of the Serine/Arginine-rich Splicing
220 Factors (SRSFs) (*25, 26*). In MYCN-amplified neuroblastoma, SRPK1 expression is elevated and
221 associated with reduced survival rates (**Fig. S2B-C**). In contrast, lower survival rates are not
222 associated with increased expression of SRPK2 nor SRPK3, indicating an increased dependency
223 on SRPK1 to drive tumour growth in MYCN-amplified tumours. Furthermore, a genome-wide
224 CRISPR study showed that loss of SRPK1 sensitizes to indisulam treatment in various solid
225 tumour cell lines (*27*). Thus, we further explored the treatment combination of SRPK1i and
226 RBM39 degraders. To this end, we assessed the synergy between indisulam and SPHINX31, a
227 known SRPK1 inhibitor(*28*). Co-treatment of SPHINX31 and indisulam exhibited synergistic
228 growth inhibition cancer across all three cell lines (**Fig. 4A**). Time-lapse cell confluency
229 monitoring in KELLY-*DCAF15*^{WT} and *DCAF15*^{KO} showed that co-treatment significantly
230 suppressed the growth of KELLY-*DCAF15*^{WT}, compared to individual drug treatments.
231 Conversely, in the absence of *DCAF15*, the combination therapy displayed similar potency to
232 SPHINX31 monotherapy (**Fig. 4B**), suggesting this interaction is DCAF15-dependent and thus
233 RBM39-dependent.

234

235 The inhibition of SRPK1 by alectinib was confirmed by enzyme activity assays which reported a
236 half-maximal inhibitory concentration (IC50) of 26nM. This inhibition is more potent than that of

237 SPHINX31 (IC50 = 375nM) with lorlatinib showing very little inhibitory action (**Fig. 4C**).
238 Notably, alectinib inhibited SRPK2 with an IC50 of 700nM while SPHINX31 showed no
239 inhibitory effect (**Fig. S2D**). Comparison of the crystal structures of the SRPK1-Alectinib and
240 SRPK1-SPHINX31 complexes confirmed that alectinib and SPHINX31 interact with the ATP-
241 binding groove of SRPK1, with reasonable affinity and occupying similar positions within the
242 binding site (**Fig. 4D** and **Fig. S3**).
243
244 SRPK1 phosphorylates SRSFs, triggering their nuclear translocation and activity in modulating
245 RNA splicing (**Fig. 4E**). Both alectinib and SPHINX31 reduced phosphorylated SRSF (p-SRSF)
246 in KELLY, HCT116 and KURAMOCHI cells (**Fig. 4F)** and decreased the nuclear-to-cytoplasmic
247 ratio of p-SRSF intensity within 4 hours in KELLY cells, while lorlatinib lacked this effect (**Fig.**
248 **4G**). SRSFs are known to promote selection of the proximal splice site in *VEGF* pre-mRNA and
249 inhibiting SRPK1 alters *VEGF* splicing to generate the *VEGF165b* isoform(*20, 29*). Treatment of
250 both alectinib and SPHINX31 resulted in a switch and increased *VEGF165b* mRNA in high-risk
251 neuroblastoma cells (**Fig. 4H**).
252
253 In conclusion, our findings reveal that alectinib is a potent inhibitor of SRPK1, consequently
254 modulating downstream function and RNA splicing through a reduction in the phosphorylation of
255 SRSF splicing factors. Notably, alectinib demonstrates more robust inhibition of SRPK1 as
256 compared to the selective inhibitor SPHINX31, an intriguing observation that could potentially
257 expedite the clinical repurposing of alectinib as an SRPK1 inhibitor.

258

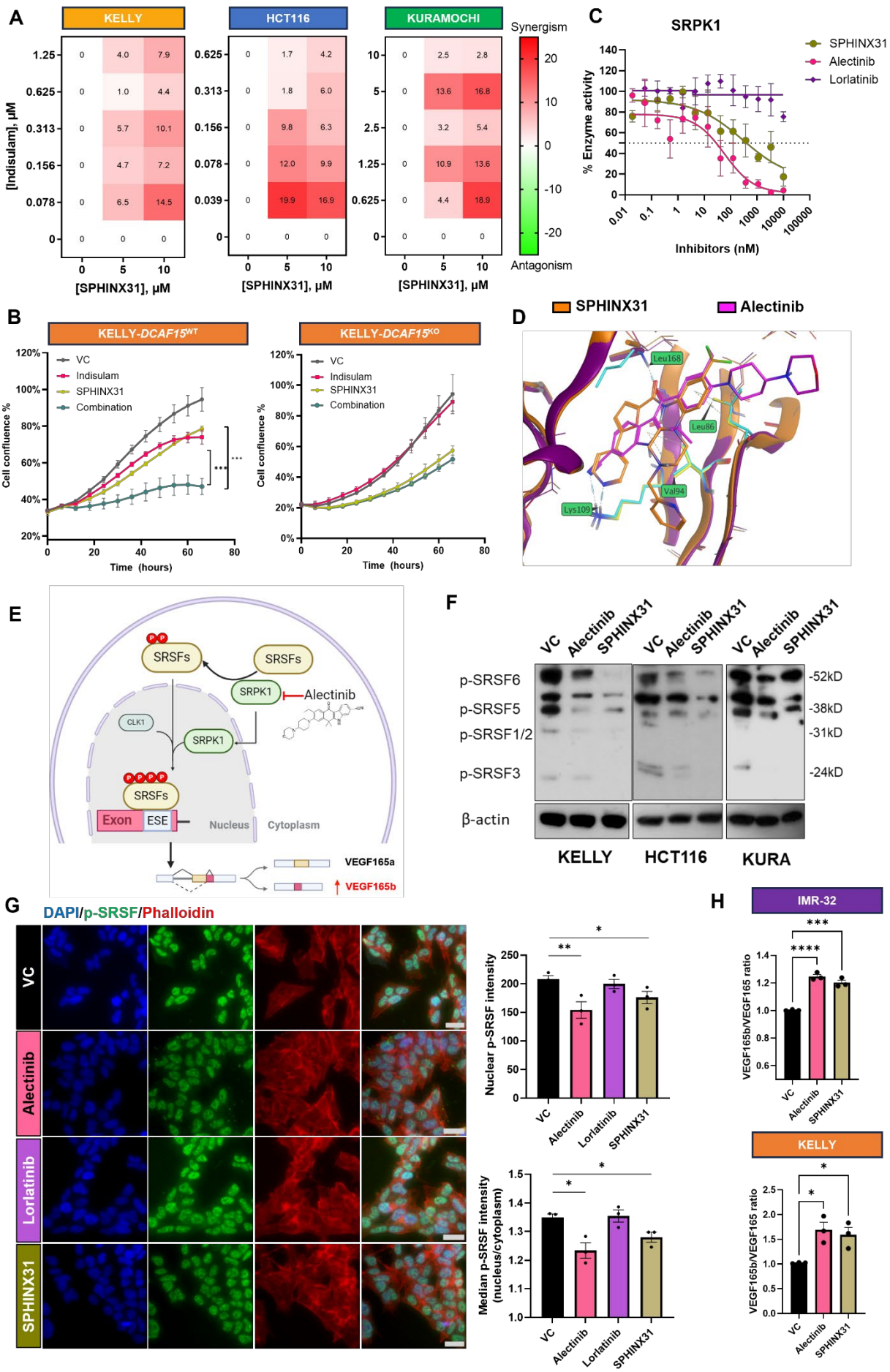
A
KELLY
HCT116
KURAMOCHI
[Indisulam], μM
[SPHINX31], μM
Synergism
Antagonism
C
SRPK1
SPHINX31
Alectinib
Lorlatinib
% Enzyme activity
Inhibitors (nM)
B
KELLY-DCAF15WT
KELLY-DCAF15KO
VC
Indisulam
SPHINX31
Combination
Cell confluence %
Time (hours)
D
SPHINX31
Alectinib
Leu168
Leu86
Val94
Lys109
E
SRSFs
SRPK1
Alectinib
CLK1
Exon
ESE
Nucleus
Cytoplasm
VEGF165a
VEGF165b
F
VC
Alectinib
SPHINX31
p-SRSF6
p-SRSF5
p-SRSF1/2
p-SRSF3
β-actin
-52kD
-38kD
-31kD
-24kD
KELLY
HCT116
KURA
G
DAPI/p-SRSF/Phalloidin
VC
Alectinib
Lorlatinib
SPHINX31
Nuclear p-SRSF intensity
Median p-SRSF intensity (nucleus/cytoplasm)
H
IMR-32
KELLY
VEGF165b/VEGF165 ratio

259 **Figure 4. SRPK1 inhibition is synergistic with indisulam in high-risk neuroblastoma.** (**A**) Indicated cell lines
260 were treated with indisulam and SPHINX31. Loewe synergy scores as indicated. (**B**) KELLY-*DCAF15*^{WT} and
261 *DCAF15*^{KO} cells were treated with indisulam and SPHINX31 individually or in combination for 72 hours. Cell
262 confluence was monitored every 6 hours using the Incucyte live cell imaging system. One-way ANOVA was used to
263 determine significance. (**C**) SRPK1 enzyme activity measured with ADP-Glo™ Kinase Assay with indicated doses of
264 compounds. (**D**) Alectinib (pink) docked into SRPK1 complexed with SPHINX31(orange). (**E**) Diagram depicting
265 Alectinib inhibition against SRPK1. Made with Biorender. (**F**) Western blotting of p-SRSF in KELLY, HCT116 and
266 KURAMOCHI post-treatment. (**G**) Immunofluorescent staining of p-SRSF in KELLY post-treatment. Nuclear
267 intensity and cytoplasmic staining intensity are calculated using DAPI and Phalloidin (F-actin) segmentation. Scale
268 bar = 20µm. (**H**) qRT-PCR of *VEGF165b* and total *VEGF165* in KELLY and IMR32 cells normalised to GAPDH. *
269 $p < 0.05$, **$p < 0.01$, ***$p < 0.001$. n = 3 independent experiments.
270

271 **Alectinib and indisulam exacerbates RNA splicing defects, increase R-loop formation and**
272 **DNA damage.**

273 Proteomic data from our previous study (*6*) showed that indisulam exposure leads to an increase
274 in protein expression of most SRSF family members (**Fig. S4A**). Here, we observed enhanced
275 nuclear translocation of p-SRSF post-indisulam treatment, which was rescued in *DCAF15*^{KO} cells
276 (**Fig. S4B-C**). These observations suggest that induction of the SRPK1/SRSF-pathway regulates
277 alternative splicing and is an adaptive response to indisulam treatment in cells compensating for
278 the loss of RBM39. RBM39 has previously been identified as a potential target of SRPK1 [25] and
279 we observed a direct interaction between RBM39 and SRPK1 in KELLY cells via Proximity
280 Ligation Assay (PLA) (**Fig. S4D**). We therefore hypothesize that the synergism observed between
281 alectinib and indisulam arises as a result of enhanced disruption of RNA splicing, and dual
282 targeting of key spliceosomal components with functional interdependence, thereby reducing the
283 opportunity for adaptive resistance.

284

285 We have previously demonstrated that degradation of RBM39 with indisulam leads to RNA
286 splicing defects preferentially targeting genes implicated in DNA damage and HR repair (*BRCA1*
287 and *RAD51D*), Fanconi Anaemia (*FANCI, FANCD2*) and Non-Homologous End Joining repair
288 pathways (*TP53BP1*, and *RIF1*)(*6, 19*). To understand the consequences of dual inhibition of
289 RBM39 and SRPK1 on these RBM39 targets, we tested the abundance of RNA splicing alterations
290 in these genes through custom PCR primer design of affected exon regions (**Fig. 5A)**. We found
291 that RBM39 targets were increasingly affected when combined with SRPK1 inhibition either with
292 alectinib or SPHINX31 in KELLY and IMR32 (**Fig. 5A-B, Fig. S5A**). This enhancement in mis-
293 splicing was not found when indisulam was combined with siALK transfection or lorlatinib (**Fig.**
294 **S5B-D**). In some cases, for example *CHK1*, the expression of the non-spliced canonical isoform
295 was almost completely lost with co-treatment of indisulam with either alectinib or SPHINX31.
296 Moreover, CHK1 protein was depleted following indisulam and alectinib combination treatment
297 (**Fig. S5E**), These data confirm a complementary function of SRPK1 and RBM39 in RNA splicing.
298 It also suggests that the synergy observed between alectinib and indisulam may be attributed to
299 the compound reduction of canonical isoform expression and enhanced functional loss in effected
300 pathways, such as DNA damage repair.

301

302 To assess whether the exacerbated impact on aberrant RNA splicing of DNA damage repair related
303 genes led to increased DNA damage, we tested the expression of γH2AX as a marker for DNA
304 double stranded breaks(*30*). γH2AX foci detected by immunofluorescence (**Fig. 5C-D**) and
305 western blot analysis (**Fig. S6A**) demonstrated a significant increase following co-treatment of
306 indisulam and alectinib compared to monotherapies. Furthermore, γH2AX expression levels did

307 not increase when indisulam was combined with lorlatinib, compared to indisulam alone (**Fig.**
308 **S6B-C**), again, demonstrating that increased DNA damage following treatment with alectinib and
309 indisulam is due to the dual targeting of RNA splicing factors, rather than ALK inhibition.
310
311 R-loops are DNA:RNA hybrids that are a product of intermediate transcription and must be
312 resolved to permit progression of replication forks (*31, 32*). R-loop accumulation results in
313 transcription-replication collisions, which generate replication stress and double-strand breaks
314 (*33*). Importantly, DNA damage repair-related factors play pivotal roles in resolving R-loops. For
315 example, BRCA1 interacts with the putative RNA helicase Senataxin (SETX), forming a complex
316 that localizes to R-loops(*34*). Several Fanconi Anemia genes recruit RNA processing enzymes to
317 resolve R-loops generated by moderate replication stress(*35*), while RIF1 facilitates replication
318 fork protection and efficient restart to maintain genome stability(*36*). Notably, SR proteins
319 regulated by SRPK1 can impede R-loop formation, ensuring faithful transcriptional elongation
320 and enhancing genomic stability(*31*). Dysregulation of these functions lead to accumulation of
321 unresolved R-loops, replication fork breakage, and genome instability (*31*).
322
323 We propose that aberrant splicing of DNA damage repair genes and inhibition of SRPK1 result in
324 R-loop accumulation, subsequent DNA damage and ultimately cell death. In KELLY cells, we
325 therefore quantitated R-loops using S9.6 antibody(*37*). Treatment with either alectinib or
326 SPHINX31 led to increased nuclear S9.6 staining indicating the accumulation of R-loops. The
327 combination treatment significantly increased R-loop formation as compared to monotherapies
328 (**Fig. 5E-F, Fig. S6D-F**). Since unresolved R loops impede the progression of replication forks,
329 causing transcription replication conflicts, and subsequent replication stress(*31, 38*), we quantified

330 the intensity of phosphorylated RPA32 serine 33 (pRPA), a marker of single-stranded DNA
331 (ssDNA) at stalled replication forks. We observed an increase following exposure to the
332 combination treatment relative as compared to monotherapy (**Fig. 5G, Fig. S6E**). To directly
333 examine altered fork dynamics, we performed DNA fibre analysis using BrdU and IdU labelling
334 (**Fig. S6G-H**). This uncovered a reduction in track length and the significantly decreased ratio of
335 IdU to BrdU when treating cells with indisulam and alectinib, indicating increased fork stalling
336 and replication stress. Collectively, these findings suggest that the combination of indisulam and
337 alectinib or SRPK1 inhibitor leads to the accumulation of unresolved R-loops, promoting
338 replication stress, and contributing to subsequent DNA damage in high-risk neuroblastoma.

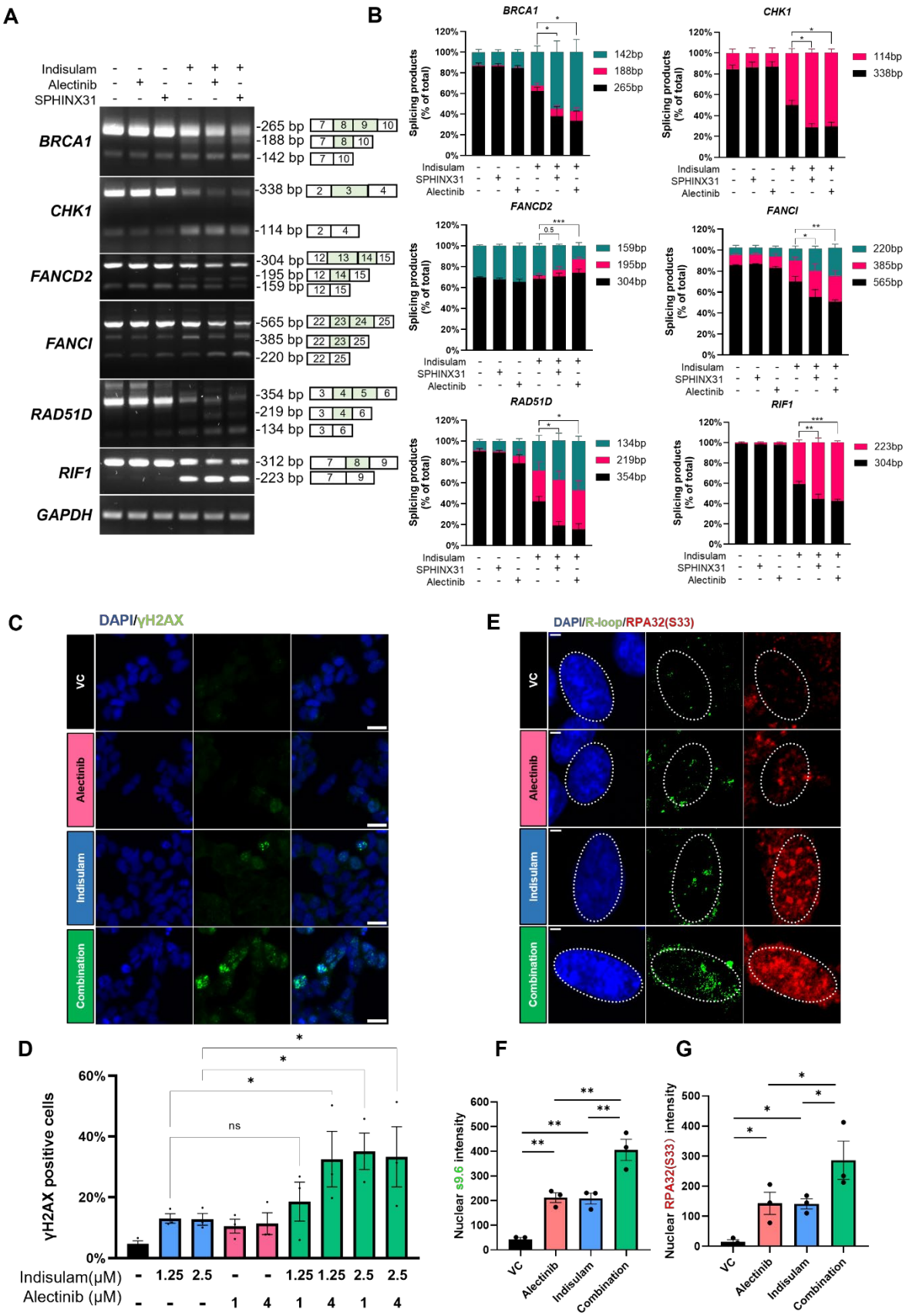
A
Indisulam
Alectinib
SPHINX31
BRCA1
-265 bp
-188 bp
-142 bp
CHK1
-338 bp
-114 bp
FANCD2
-304 bp
-195 bp
-159 bp
FANCI
-565 bp
-385 bp
-220 bp
RAD51D
-354 bp
-219 bp
-134 bp
RIF1
-312 bp
-223 bp
GAPDH
B
BRCA1
142bp
188bp
265bp
CHK1
114bp
338bp
FANCD2
159bp
195bp
304bp
FANCI
220bp
385bp
565bp
RAD51D
134bp
219bp
354bp
RIF1
223bp
304bp
Splicing products (% of total)
C
DAPI/γH2AX
VC
Alectinib
Indisulam
Combination
D
γH2AX positive cells
ns
Indisulam(μM)
Alectinib (μM)
E
DAPI/R-loop/RPA32(S33)
F
Nuclear s9.6 intensity
G
Nuclear RPA32(S33) intensity

340 **Figure 5. Combination of indisulam and alectinib induce DNA damage, R-loop accumulation and replication**
341 **stress.** (**A**) PCR validation of exon skipping events in DDR-related genes (representative image of n=3). *GAPDH* was
342 included as a control. (**B**) Densitometry analysis of alternative splicing products, Two-way ANOVA was used to detect
343 the significance. (**C-D**) Immunofluorescence staining of γH2AX in KELLY cells treated with indisulam in
344 combination of alectinib. Representative images of KELLY treated with 4μM alectinib and 1.25μM indisulam are
345 shown. Scale bars = 20μm. Nuclear foci >5 indicates positive cells. n=3 independent experiments. (**E**) Representative
346 images for nuclear S9.6 and RPA32 (S33) staining in KELLY cells, n = 3 independent experiments, Scale
347 bars = 2.5μm. (**F-G**) Quantification of nuclear S9.6 intensity (F) and pRPA32 (G) intensity in KELLY cells. Cells
348 were treated with 4μM alectinib monotherapy or with 1.25μM indisulam; nuclear signal intensity were measured by
349 merging to DAPI; n>300 cells from 3 independent experiments were quantified. Significance was analysed among
350 the median values.
351

352 **Combination of indisulam and alectinib improves survival in a Th-MYCN/ALK^{F1174L}**
353 **neuroblastoma model**

354 Gain-of-function mutations in ALK account for 10-15% of high-risk neuroblastoma (*9*). ALK
355 inhibitors have been shown to be safe and effective in treating ALK-driven neuroblastoma in a
356 Phase I trial(*39, 40*), and are currently being investigated in several Phase III trials(*39, 41, 42*),
357 highlighting their potential for clinical use in ALK-positive neuroblastoma. Considering the clinic
358 relevance and benefit, we used an allograft mouse model implanted with Th-MYCN/ALK^{F1174L}
359 tumour cells derived from genetically engineered mouse models (GEMMs) (**Fig.6A**).
360

361 Tumour-bearing mice were treated (indisulam 10mg/kg, alectinib 40mg/kg or combination) for 2-
362 weeks with a 45-day follow-up. Both monotherapies significantly enhanced survival however all
363 alectinib treated mice relapsed on treatment and 5/8 mice in the indisulam monotherapy group
364 relapsed after withdrawal of treatment. Complete tumour regression without subsequent relapse

365 resulting in a 100% survival rate were reported in the combination group (**Fig. 6B-C**) consistent
366 with the increased efficacy in-vitro.
367 Tumour samples were collected for pharmacodynamic analysis after 3 days of treatment. Western
368 blotting showed a clear depletion of RBM39 following indisulam and combination therapy,
369 confirming the on-target effect of indisulam (**Fig. 6D**). Furthermore, treatment with 10 mg/kg
370 indisulam reduced MYCN expression, as previously reported by Singh et al (*43*), suggesting a
371 potential link between RBM39 inhibition and suppression of MYCN (**Fig. 6D**). Additionally, a
372 decrease in p-ALK **(Fig. S7A)**, and a reduction in p-SRSF (**Fig. 6F**) confirmed the on-target effects
373 of alectinib on SRPK1 and ALK. Double strand breaks measured by accumulation of γH2AX foci,
374 were increased in combination therapies (**Fig. 6G**), in line with our observations *in-vitro.* However,
375 indisulam alone did not significantly induce γH2AX accumulation, possibly due to the transient
376 nature of γH2AX focus formation during the DNA damage response. However, clear nuclear
377 fragmentation was observed in mice treated with indisulam and combination therapy (**Fig. 6G**).
378 Importantly, no significant weight loss was observed during the trial, indicating no significant
379 toxicity (**Fig. S7B)**, and we observed no significant RBM39 loss in other organs after 3-day
380 treatment (**Fig. S7C**).
381 Taken together, these data confirm that in neuroblastoma the therapeutic benefit of RBM39-
382 depleting agents can be enhanced through combination with SRPK1 inhibitors, such as alectinib.
383 This study provides proof-of concept for the co-targeting of functionally interdependent splicing
384 factors using repurposed clinical agents to more effectively target aggressive childhood cancers
385 such as neuroblastoma. The strategy could apply more widely to other oncogene-driven cancers
386 that exhibit a high dependency on faithful splicing of mRNA.

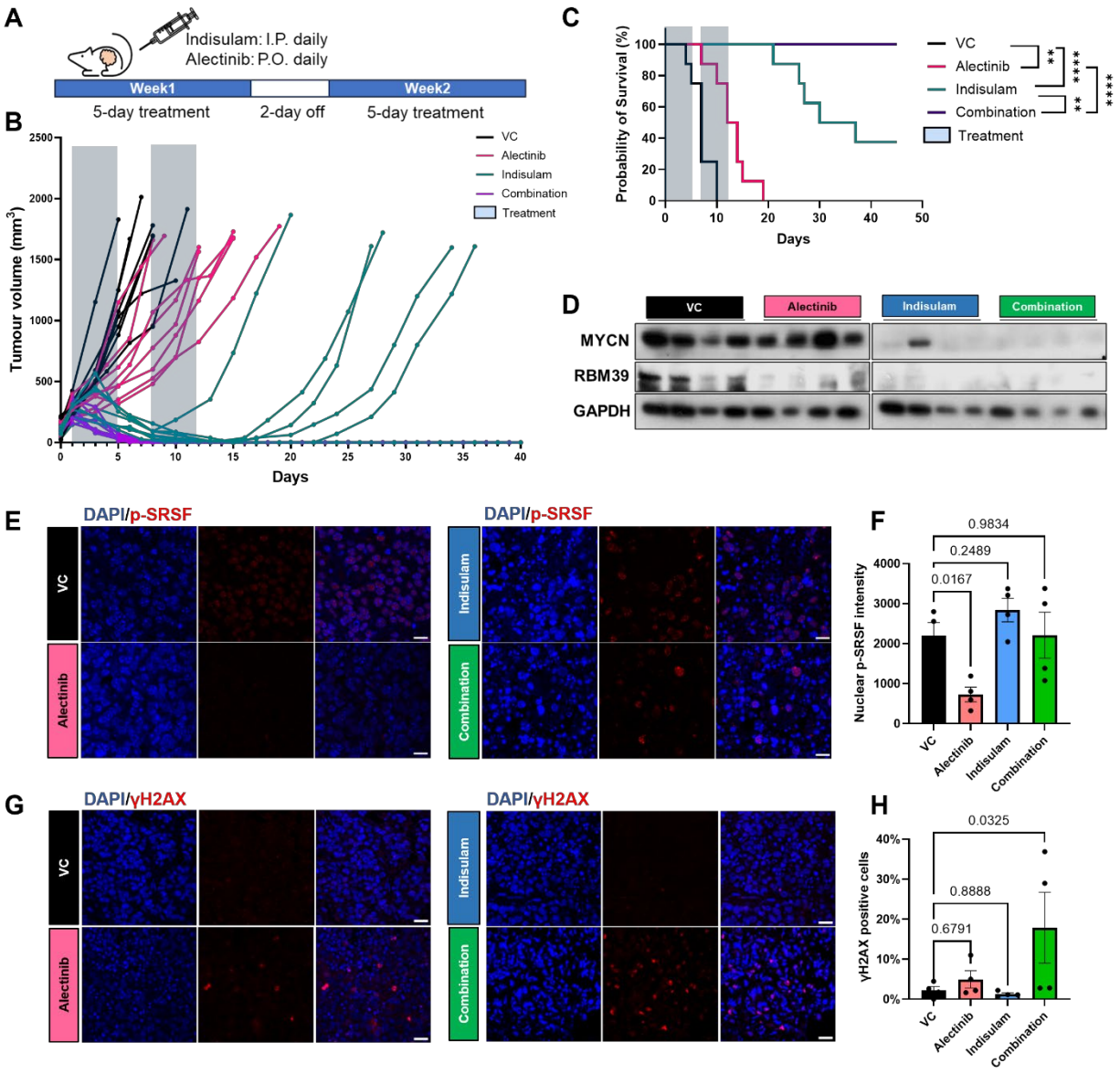

387

388 **Figure.6. Combination of indisulam and alectinib suppress neuroblastoma tumour growth.** (**A**) Th-
389 ALK^{F1174L}/Th-MYCN GEMM tumour cells were injected into a cohort of mice subcutaneously, intravenous (i.v.)
390 administration of 10 mg/kg of indisulam and oral gavage (p.o.) 40 mg/kg of alectinib for 2 weeks with 5 days on and
391 2 days off. (**B**) Tumour volume measured 3 times a week until the humane end-point was reached. Cyan shade
392 indicates the treatment period. n = 8 for each group. (**C**) Survival plot of mice bearing Th-ALK^{F1174L}/Th-MYCN
393 allografts treated with vehicle or alectinib or indisulam or combination therapy. (**D**) Western blotting in tumour tissues
394 after administration of vehicle or alectinib or indisulam or combination therapy for 3 days (n = 4 per group). (**E-H**)
395 Immunofluorescence staining was performed on tumour sections, with DAPI used for nuclear staining. Nuclear p-

396 SRSF intensity (E-F) was measured by merging to DAPI. Nuclear γH2AX (G-H) foci >5 indicates positive cells. Scale
397 bar = 20 μm. n.s. not significant, * $p < 0.05$, ** $p<0.01$, *** $p < 0.001$, **** $p < 0.0001$.
398

399 **DISCUSSION**

400 Indisulam has been recently identified as a molecular glue capable of regulating RNA alternative
401 splicing(*2*). By inducing splicing errors of genes in key oncogenic pathways, indisulam and other
402 spliceosomal inhibitors may render cancer cells susceptible to additional disruptions caused by
403 other anticancer drugs. Thus, it holds potential for implementation as combination therapy. We
404 performed extensive drug screens with FDA-approved anticancer agents which revealed several
405 potential drug-drug interactions with indisulam. Notably, the synergy between indisulam and
406 PARP inhibitors, also observed in our screens, has been corroborated by other studies in high-
407 grade ovarian carcinoma(*19*), has also been verified independently in colorectal cancer, and breast
408 cancer(*44*), giving confidence in our screening approach. Our study also highlights the fact that
409 such screens can reveal beneficial pharmacological interactions based on off-target effects (targets
410 other than the primary focus of clinical development), presenting novel rationales for drug
411 repurposing.
412

413 High-risk neuroblastoma, which constitutes about 15% of all neuroblastoma cases, is characterized
414 by aggressive behaviour and poor prognosis(*10*). Gain-of-function mutations in ALK account for
415 10-15% of primary tumours (*9*), hence a number of trials have investigated the use of alectinib and
416 other ALK inhibitors in this clinical setting. While the more selective ALK inhibitor loratinib has
417 shown greater traction for the treatment of mutant ALK-driven neuroblastoma(*39*), treatment
418 resistance remains a significant clinical challenge(*45*). Our study demonstrates that the activity of
419 alectinib against SRPK1 can be exploited therapeutically in combination with other spliceosomal

420 inhibitors. This presents an interesting strategy to treat patients with emerging resistance to ALK
421 inhibitor therapy, including in lung cancer where alectinib has demonstrated much greater clinical
422 use(*41*) and beyond into other cohorts irrespective of ALK status. While other inhibitors of SRPKs
423 and related SRSF regulators such as Cirtuvivint(*46*) and TG-003(*47*) are currently in early
424 development, the fact that an established therapeutic tool can be repurposed in this way could
425 accelerate the clinical testing of SRPK1/2 inhibition and co-targeting of splicing factors as an anti-
426 cancer treatment strategy, particularly in tumours where an ALK inhibitor might normally be
427 indicated.
428
429 While we have successfully demonstrated the principle of co-targeting functionally interdependent
430 splicing as an anticancer strategy, several resulting questions arise. Our investigation into the
431 functional consequences of combined RBM39 degradation and SRPK1 inhibition underscores
432 their interdependency in regulating alternative splicing, but it is not yet clear if RBM39 is a direct
433 target of SPRK1 as has been suggested by global interaction profiling (*48*) and our co-localisation
434 experiments. More broadly, we need further investigation to understand the interactions and co-
435 regulation of different splicing factors that are also cancer targets such as RBM39 and SPRK1,
436 and to develop more detailed mechanistic models of how these regulate alternative splicing
437 together.
438
439 Interestingly, when alectinib/SRPK1 inhibition was used alone, there was no detectable induction
440 of DDR genes mis-splicing observed in neuroblastoma. This is in contrast to interference with
441 RBM39 function(*19*) and what we might expect if the effect of alectinib was acting purely through
442 direct regulation of RBM39 activity and the mis-splicing of a specific gene family. As with the

443 targeting of spliceosomal components in general, it is unclear if the sequelae of accumulating R
444 loops, cell cycle arrest, DNA damage and eventual cell death that we observe in combined
445 SRPK1/RBM39 interference are lineage-dependent, result from mis-splicing and loss of function
446 of a select set of genes, or the accumulative impact of hundreds or even thousands of splicing
447 events within a functional pathway. Further work to resolve such mechanistic questions will be
448 important to understand what the most relevant pharmacodynamic readouts will be for future
449 discovery experiments and which predictive biomarkers can best identify patients most likely to
450 benefit from such combinations (i.e. for stratification).
451
452 In summary, the present study elucidates a novel therapeutic approach utilizing the combination
453 of indisulam and alectinib in high-risk neuroblastoma, and our results support a model in which
454 co-treatment indisulam and alectinib synergistically impacts RNA splicing through simultaneous
455 RBM39 degradation and SRPK1 inhibition. This dual RNA splicing interference exacerbates
456 splicing errors in key genes involved in DNA damage repair and in R-loop resolution, leading to
457 R-loop accumulation and increased DNA damage. These events eventually result in cellular
458 apoptosis and growth inhibition in high-risk neuroblastoma *in vitro*, as well as suppression of
459 tumour growth *in vivo*. These insights shed new light on translating research on spliceosome
460 inhibition into clinical applications, ultimately aiming to improve the prognosis for patients with
461 high-risk neuroblastoma.
462

463 **MATERIALS AND METHODS**

464 **Study design**

465 The objectives of this study were to identify the synergistic mechanism of action and therapeutic
466 potential of indisulam combined with alectinib in high-risk neuroblastoma. We conducted drug
467 screens in cancer cell lines and confirmed synergy in neuroblastoma models. Genetic and
468 pharmacological experiments determined whether dual interference with RNA splicing—via
469 RBM39 degradation and SRPK1 inhibition—could exacerbate RNA splicing defects in DNA
470 damage repair genes, leading to enhanced DNA damage, R-loop accumulation, apoptosis, and
471 tumor suppression. Animals were treated with indisulam and alectinib for two weeks. Sample sizes
472 were based on prior experience with model growth profiles, providing sufficient statistical power
473 to detect differences. Tumour volumes were measured every 2 to 3 days, and animals were
474 euthanized upon reaching humane endpoints or impaired health criteria.

475

476 **Cell lines and cell culture**

477 Human neuroblastoma cell lines were cultured in were cultured in MEM (Gibco™) supplemented
478 with 10% fetal bovine serum (FBS), 1% penicillin/streptomycin (P/S), 1mM sodium pyruvate and
479 2 mM L-Glutamine. KURAMOCHI was maintained in Dulbecco's Modified Eagle Medium
480 (DMEM, Gibco™), supplemented with 10% FBS, 2 mM of L-Glutamine, 5.6 mM Glucose and
481 1%Penicillin-Streptomycin. HCT116 was cultured in Roswell Park Memorial Institute (RPMI)
482 1640 Medium (Gibco™) supplemented with 10% FBS, 2 mM L-Glutamine, 1% Penicillin-
483 Streptomycin. All cells were authenticated by Public Health England and regularly tested for
484 mycoplasma contamination. All cells were maintained at 37 °C with 5% CO2 in a controlled
485 environment.

486

487 **Sulforhodamine B (SRB) assay**

488 Cells at the experiment's endpoint were fixed with 10% (w/v) cold trichloroacetic acid (TCA)
489 (Sigma) and stained with 0.4% protein-bound SRB dye for 30 minutes. Excess dye was removed
490 by washing the cells three times with 1% (v/v) acetic acid. The bound SRB dye was then
491 solubilized in 10 mM Tris-Base solution, and the optical density (OD) was measured at 565 nm
492 using a ClarioStar microplate reader (BMG Labtech). The results were normalized to the vehicle
493 control values, with the control set as 100%.

494

495 **Synergy analysis**

496 Cell growth inhibition was assessed by SRB assay after 72 hours of drug exposure. The inhibition
497 was calculated by normalizing the mean OD values of each treatment group to vehicle control.
498 The Loewe additivity model was used to describe the interaction between two agents[32]. Cells
499 were treated with specific concentration matrices of the drugs, and cell growth data were analysed
500 using SynergyFinder 2.0 (https://synergyfinder.fimm.fi) to compute synergy scores. A synergy
501 score greater than 10 indicates synergism, a score between -10 and 10 represents additivity, and a
502 score below -10 reflects antagonism.

503

504 **Western blotting**

505 Whole-cell lysates were prepared using RIPA buffer (Sigma Aldrich) with 1% HALT protease and
506 phosphatase inhibitor cocktail (Thermo Scientific). Equal amounts of protein from each sample
507 were separated on a 4-20% Bis-Tris SurePAGE gel (GenScript) and then transferred onto PVDF
508 membranes. The membranes were blocked with 5% milk for 1 hour at room temperature, followed
509 by an overnight incubation at 4°C with CHK1 (#2360, Cell Signaling Technology), p-CHK1

510 (#2348, Cell Signaling Technology), γH2AX (#05–636, Sigma-Aldrich). After washing, the
511 membranes were incubated with horseradish peroxidase (HRP)-conjugated secondary antibody for
512 1 hour at room temperature. Chemiluminescent detection was performed using SuperSignal West
513 Pico PLUS Chemiluminescent Substrate (Thermo Scientific).

514

515 **End-point and quantification PCR reactions**

516 1500ng RNA was utilized for reverse transcription, employing the High-Capacity RNA-to-
517 cDNA™ Kit (Applied Biosystems) in accordance with the provided instructions. The resulting
518 cDNA templates were subsequently employed for qPCR using thePowerTrack SYBR Green
519 Master Mix (Applied Biosystems) or End-point PCR utilizing the Q5® High-Fidelity PCR Kit
520 (New England Biolab). Primers were specifically designed to investigate alternative splicing
521 events of the targeted genes. The PCR products were separated by electrophoresis using 2%
522 agarose gels with SYBRsafe DNA gel stain, and the images were captured for densitometry
523 analysis by Fiji V2.0.0.

Target genes	Primer (5' to 3')	Tm
BRCA1	AACTCTGAGGACAAAGCAGC CTTCTCAGTGGTGTTCAAATC	62
CHK1	GTGGAAGACTGGGACTTGGT ACCCCTGCCATGAGTTGATG	68
FANCD2	CGGTTACAGGCTTCCCAAGT GCTGTTCTTGAATGCAGCCT	67
FANCI	GAGTCAGGCCGAGAAGGTTC CAACGGCAGCAGGTTTCTC	68
RAD51D	TGGCTCAGTTCTCGGCTTT	66

	AGATGTCAAATGCATGCACCA	
TP53BP1	GCTGTTGCTGAGTCTGTTGC TGCGTACTTCCCGGATTGTT	68
RIF1	AGGTGGGCAAAACTGGTCAT TGGGTGCTCCACTACGAAAT	67
VEGF165b	AAGAAAATCCCTGTGGGCCTT TGGTGAGAGATCTGCAAGTACGTT	60
VEGF165	AGAGCAAGACAAGAAAATCC TACAAACAAATGCTTTCTCC	53
GAPDH	GGCTGCTTTTAACTCTGG GGAGGGATCTCGCTCC	62

524 **Immunofluorescence staining**

525 KELLY cells were fixed using 4% paraformaldehyde (PFA) for 15 minutes, followed by
526 permeabilization with 0.1% Triton-X100 for 20 minutes. The cells were then blocked with 5%
527 BSA in PBS-T for 30mins at room temperature. Subsequently, they were incubated overnight at
528 4°C with anti-phosphoepitope SR proteins antibody (1:100, #MABE50, Sigma-Aldrich) or
529 γH2AX (1:500, #05–636, Sigma-Aldrich) in blocking buffer. Following this, cells were washed
530 before staining with a mix of Alexa Fluor 488-conjugated goat anti-mouse antibody (1:500,
531 AF488, Thermo Scientific), DAPI (1µg/ml, #40043, Biotium,), and Phalloidin-647 (1:50, #8940S,
532 Cell Signaling Technology) for 1 hour at room temperature. The cells were washed again three
533 times with PBS-T before imaging with an INCell Analyzer 1000 microscope (GE Healthcare) at
534 20x magnification.

535 S9.6 (1:250, MABE1095, Sigma-Aldrich) and phospho RPA32-S33 (1:250, #NB100-544, Novus)
536 were detected in KELLY cells fixed with cold methanol at -20°C for 10 minutes and slides were
537 imaged using the Aurox laser-free confocal microscope. To confirm the specificity of the S9.6

538 antibody, RNase H (Ribonuclease H, 1:100, #M0297S, NEB) was applied to the fixed cells before
539 antibody incubation.

540 Image analysis was performed using Cell Profiler V4.2.6, with nuclear regions masked by DAPI
541 staining and cytoplasmic regions masked by Phalloidin staining, excluding areas overlapping with
542 DAPI.

543

544 **SRPK1/2 kinase activity assay**

545 The SRPK1 Kinase Enzyme System (#VA7558, Promega) and SRPK2 Kinase Enzyme System
546 (#VA7561, Promega) were utilised with the ADP-Glo™ Kinase Assay (#V6930, Promega),
547 following the manufacturer's protocol. Briefly, 1 µl of inhibitor, diluted in 1X kinase reaction
548 buffer, was added to the wells of a 384-well low-volume plate and combined with 8 ng of SRPK1
549 enzyme. Following this, 2 µl of a substrate/ATP mixture (100 µM ATP, 0.1 µg/µl MBP) was
550 added. The reaction was incubated at room temperature for 1 hour. After incubation, 5 µl of ADP-
551 Glo™ Reagent was added to each well, and the plate was incubated at room temperature for 40
552 minutes. Subsequently, 10 µl of Kinase Detection Reagent was added, and the plate was incubated
553 for an additional 30 minutes. Luminescence was recorded.

554

555 **Proximity Ligation Assay (PLA)**

556 The Duolink® Proximity Ligation Assay (PLA) was used to detect protein-protein interactions in
557 KELLY cells. Samples were fixed with 4% paraformaldehyde, permeabilised with 0.1% Triton X-
558 100, and blocked with the Duolink® blocking solution. Primary antibodies against RBM39 (1:500,
559 67420, Proteintech) and SRPK1 (1:250, ab90527, Abcam) were applied overnight at 4°C. Species-

560 specific PLA probes (Sigma-Aldrich) were added, followed by ligation and rolling-circle
561 amplification according to the manufacturer's instructions.

562

563 **DNA fibre analysis**

564 Cells were sequentially pulse-labeled with 10 μM BrdU and 200 mM IdU for 30 minutes each.
565 KELLY cells were spotted on SuperFrost slides, air-dried for 5 minutes, and lysed with a buffer
566 (200 mM Tris-HCl, pH 7.5, 50 mM EDTA, 0.5% SDS) to release DNA. After air-drying for 5
567 minutes, the slides were tilted to allow DNA to spread, then dried, fixed in 75% methanol/25%
568 acetic acid, and treated with 2.5M HCl for 1 hour to denature the DNA. After PBS washes, slides
569 were blocked with 1% BSA in PBS-T for 1 hour. BrdU was detected by incubating slides with rat
570 anti-BrdU antibody (1:50, ab6326, Abcam) followed by AF647-conjugated secondary antibody
571 (1:100, A21247, Invitrogen). IdU was labeled with mouse anti-BrdU antibody (1:50, #BD347580)
572 and AF488-conjugated secondary antibody (1:100, #A11001, Invitrogen). Slides were mounted
573 and imaged using a laser-free confocal microscope, with DNA track lengths measured in Fiji V2.0.

574

575 **In vivo allograft model of neuroblastoma**

576 Syngeneic tumours derived from TH-MYCN/ALK^{F1174L} genetically engineered mouse models
577 (GEMMs), were implanted into immune competent 129×1/SvJ mice. Treatment began when the
578 implanted tumours reached a volume of over 200 mm³. The dosing schedule continued for 2 weeks,
579 with daily administration for 5 days followed by 2 days off. Alectinib was dissolved in saline
580 containing 40% PEG300, 10% DMSO, and 5% Tween, and was administered orally at a dose of
581 10 μL/kg. Indisulam was dissolved in saline with 3.5% DMSO and 6.5% Tween80 and was

582 administered intravenously at a dose of 5 µL/kg. Tumour tissues were excised two hours after the
583 final dose of each compound. Half of the tumour was fixed in 4% PFA, while the other half was
584 snap-frozen for subsequent analysis.

585

586 **Immunoassays on tissue samples**

587 Snap frozen tumours were lysed in 5% CHAPS buffer and western blotting was carried out for
588 RBM39 (#67420, Proteintech) ERK1/2 (#4695 Cell Signaling Technology), pERK1/2 (#9101,
589 Cell Signaling Technology), phosphoepitope SR proteins (#MABE50, Sigma-Aldrich) and
590 GAPDH (#2118, Cell Signaling). ALK Meso Scale Discovery® immunoassays were performed
591 as previously described(*49*)

592

593 **Immunofluorescence on tissue sections**

594 Tumours were processed using an ASP300S tissue processor (Leica) following the manufacturer's
595 guidelines. Sections were deparaffinized and rehydrated using Xylene and a graded series of
596 alcohol, followed by a 5-minute rinse in water. They were then boiled in 1% citric-acid buffer for
597 20 minutes and allowed to cool to room temperature. The sections were blocked for 1 hour in TBS
598 with 0.01% Triton (TBST) and 5% BSA. Afterwards, γH2AX antibody (#9718, Cell Signaling
599 Technology) was applied at a 1:100 dilution in blocking buffer and incubated overnight at 4°C.
600 After 3 TBST washes, a secondary Alexa Fluor 568 goat anti-rabbit antibody (1:1000) was
601 incubated at room temperature for 1 hour. Images were captured using a confocal microscope
602 (LSM700, LSM T-PMT) and processed with ZEN2009 software (Black version, Zeiss).

603

604 **Statistical Analysis**

605 Statistical analyses were conducted using GraphPad Prism 10. For normally distributed data, a
606 Student's t-test was used for two-group comparisons, while one-way ANOVA with multiple
607 comparisons was applied to three or more groups. Two-way ANOVA with multiple comparisons
608 was used for multi-group analyses involving two factors. Specific statistical details are provided
609 in the figure legends.

610

611 **List of Supplementary Materials**

612 Fig S1 to S7 for multiple supplementary figures

613 Table S1 for supplementary table

614 **References and Notes**

615 1. A. A. Patel, J. A. Steitz, Splicing double: insights from the second spliceosome. *Nat Rev Mol Cell Biol* **4**,
616 960-970 (2003).
617 2. T. Han, M. Goralski, N. Gaskill, E. Capota, J. Kim, T. C. Ting, Y. Xie, N. S. Williams, D. Nijhawan,
618 Anticancer sulfonamides target splicing by inducing RBM39 degradation via recruitment to DCAF15.
619 *Science* **356**, (2017).
620 3. C. Xu, X. Chen, X. Zhang, D. Zhao, Z. Dou, X. Xie, H. Li, H. Yang, Q. Li, H. Zhang, C. Di, RNA-binding
621 protein 39: a promising therapeutic target for cancer. *Cell Death Discov* **7**, 214 (2021).
622 4. T. Uehara, Y. Minoshima, K. Sagane, N. H. Sugi, K. O. Mitsuhashi, N. Yamamoto, H. Kamiyama, K.
623 Takahashi, Y. Kotake, M. Uesugi, A. Yokoi, A. Inoue, T. Yoshida, M. Mabuchi, A. Tanaka, T. Owa,
624 Selective degradation of splicing factor CAPERalpha by anticancer sulfonamides. *Nat Chem Biol* **13**, 675-
625 680 (2017).
626 5. J. Bojko, M. Kollareddy, M. Szemes, J. Bellamy, E. Poon, A. Moukachar, D. Legge, E. E. Vincent, N.
627 Jones, S. Malik, A. Greenhough, A. Paterson, J. H. Park, K. Gallacher, L. Chesler, K. Malik, Spliceosomal

628 vulnerability of MYCN-amplified neuroblastoma is contingent on PRMT5-mediated regulation of
629 epitranscriptomic and metabolomic pathways. *Cancer Lett* **604**, 217263 (2024).
630 6. A. Nijhuis, A. Sikka, O. Yogev, L. Herendi, C. Balcells, Y. Ma, E. Poon, C. Eckold, G. N. Valbuena, Y.
631 Xu, Y. Liu, B. M. da Costa, M. Gruet, C. Wickremesinghe, A. Benito, H. Kramer, A. Montoya, D. Carling,
632 E. J. Want, Y. Jamin, L. Chesler, H. C. Keun, Indisulam targets RNA splicing and metabolism to serve as a
633 therapeutic strategy for high-risk neuroblastoma. *Nat Commun* **13**, 1380 (2022).
634 7. A. Salib, N. Jayatilleke, J. A. Seneviratne, C. Mayoh, K. De Preter, F. Speleman, B. B. Cheung, D. R.
635 Carter, G. M. Marshall, MYCN and SNRPD3 cooperate to maintain a balance of alternative splicing events
636 that drives neuroblastoma progression. *Oncogene* **43**, 363-377 (2024).
637 8. S. Singh, W. Quarni, M. Goralski, S. Wan, H. Jin, L. A. Van de Velde, J. Fang, Q. Wu, A. Abu-Zaid, T.
638 Wang, R. Singh, D. Craft, Y. Fan, T. Confer, M. Johnson, W. J. Akers, R. Wang, P. J. Murray, P. G.
639 Thomas, D. Nijhawan, A. M. Davidoff, J. Yang, Targeting the spliceosome through RBM39 degradation
640 results in exceptional responses in high-risk neuroblastoma models. *Sci Adv* **7**, eabj5405 (2021).
641 9. K. K. Matthay, J. M. Maris, G. Schleiermacher, A. Nakagawara, C. L. Mackall, L. Diller, W. A. Weiss,
642 Neuroblastoma. *Nat Rev Dis Primers* **2**, 16078 (2016).
643 10. N. Bechmann, F. Westermann, G. Eisenhofer, HIF and MYC signaling in adrenal neoplasms of the neural
644 crest: implications for pediatrics. *Front Endocrinol (Lausanne)* **14**, 1022192 (2023).
645 11. J. Otte, C. Dyberg, A. Pepich, J. I. Johnsen, MYCN Function in Neuroblastoma Development. *Front Oncol*
646 **10**, 624079 (2020).
647 12. Y. Chen, J. Takita, Y. L. Choi, M. Kato, M. Ohira, M. Sanada, L. Wang, M. Soda, A. Kikuchi, T. Igarashi,
648 A. Nakagawara, Y. Hayashi, H. Mano, S. Ogawa, Oncogenic mutations of ALK kinase in neuroblastoma.
649 *Nature* **455**, 971-974 (2008).
650 13. A. T. Shaw, L. Gandhi, S. Gadgeel, G. J. Riely, J. Cetnar, H. West, D. R. Camidge, M. A. Socinski, A.
651 Chiappori, T. Mekhail, B. H. Chao, H. Borghaei, K. A. Gold, A. Zeaiter, W. Bordogna, B. Balas, O. Puig,
652 V. Henschel, S. I. Ou, i. study, Alectinib in ALK-positive, crizotinib-resistant, non-small-cell lung cancer: a
653 single-group, multicentre, phase 2 trial. *Lancet Oncol* **17**, 234-242 (2016).

654 14. M. W. Alam, M. Borenas, D. E. Lind, D. Cervantes-Madrid, G. Umapathy, R. H. Palmer, B. Hallberg,
655 Alectinib, an Anaplastic Lymphoma Kinase Inhibitor, Abolishes ALK Activity and Growth in ALK-
656 Positive Neuroblastoma Cells. *Front Oncol* **9**, 579 (2019).
657 15. J. Lu, S. Guan, Y. Zhao, Y. Yu, S. E. Woodfield, H. Zhang, K. L. Yang, S. Bieerkehazhi, L. Qi, X. Li, J.
658 Gu, X. Xu, J. Jin, J. A. Muscal, T. Yang, G. T. Xu, J. Yang, The second-generation ALK inhibitor alectinib
659 effectively induces apoptosis in human neuroblastoma cells and inhibits tumor growth in a TH-MYCN
660 transgenic neuroblastoma mouse model. *Cancer Lett* **400**, 61-68 (2017).
661 16. A. Zafar, W. Wang, G. Liu, X. Wang, W. Xian, F. McKeon, J. Foster, J. Zhou, R. Zhang, Molecular
662 targeting therapies for neuroblastoma: Progress and challenges. *Med Res Rev* **41**, 961-1021 (2021).
663 17. P. J. Houghton, R. T. Kurmasheva, Challenges and Opportunities for Childhood Cancer Drug
664 Development. *Pharmacol Rev* **71**, 671-697 (2019).
665 18. O. Anczukow, A. R. Krainer, The spliceosome, a potential Achilles heel of MYC-driven tumors. *Genome*
666 *Med* **7**, 107 (2015).
667 19. Y. Xu, S. Spear, Y. Ma, M. P. Lorentzen, M. Gruet, F. McKinney, Y. Xu, C. Wickremesinghe, M. R.
668 Shepherd, I. McNeish, H. C. Keun, A. Nijhuis, Pharmacological depletion of RNA splicing factor RBM39
669 by indisulam synergizes with PARP inhibitors in high-grade serous ovarian carcinoma. *bioRxiv*,
670 2023.2001.2018.524417 (2023).
671 20. J. M. Hatcher, G. Wu, C. Zeng, J. Zhu, F. Meng, S. Patel, W. Wang, S. B. Ficarro, A. L. Leggett, C. E.
672 Powell, J. A. Marto, K. Zhang, J. C. Ki Ngo, X. D. Fu, T. Zhang, N. S. Gray, SRPKIN-1: A Covalent
673 SRPK1/2 Inhibitor that Potently Converts VEGF from Pro-angiogenic to Anti-angiogenic Isoform. *Cell*
674 *Chem Biol* **25**, 460-470 e466 (2018).
675 21. C. I. BLISS, THE TOXICITY OF POISONS APPLIED JOINTLY1. *Annals of Applied Biology* **26**, 585-
676 615 (1939).
677 22. M. Uhlen, E. Bjorling, C. Agaton, C. A. Szigyarto, B. Amini, E. Andersen, A. C. Andersson, P. Angelidou,
678 A. Asplund, C. Asplund, L. Berglund, K. Bergstrom, H. Brumer, D. Cerjan, M. Ekstrom, A. Elobeid, C.
679 Eriksson, L. Fagerberg, R. Falk, J. Fall, M. Forsberg, M. G. Bjorklund, K. Gumbel, A. Halimi, I. Hallin, C.
680 Hamsten, M. Hansson, M. Hedhammar, G. Hercules, C. Kampf, K. Larsson, M. Lindskog, W. Lodewyckx,
681 J. Lund, J. Lundeberg, K. Magnusson, E. Malm, P. Nilsson, J. Odling, P. Oksvold, I. Olsson, E. Oster, J.

682 Ottosson, L. Paavilainen, A. Persson, R. Rimini, J. Rockberg, M. Runeson, A. Sivertsson, A. Skollermo, J.
683 Steen, M. Stenvall, F. Sterky, S. Stromberg, M. Sundberg, H. Tegel, S. Tourle, E. Wahlund, A. Walden, J.
684 Wan, H. Wernerus, J. Westberg, K. Wester, U. Wrethagen, L. L. Xu, S. Hober, F. Ponten, A human protein
685 atlas for normal and cancer tissues based on antibody proteomics. *Mol Cell Proteomics* **4**, 1920-1932
686 (2005).
687 23. N. R. Infarinato, J. H. Park, K. Krytska, H. T. Ryles, R. Sano, K. M. Szigety, Y. Li, H. Y. Zou, N. V. Lee,
688 T. Smeal, M. A. Lemmon, Y. P. Mosse, The ALK/ROS1 Inhibitor PF-06463922 Overcomes Primary
689 Resistance to Crizotinib in ALK-Driven Neuroblastoma. *Cancer Discov* **6**, 96-107 (2016).
690 24. H. Sakamoto, T. Tsukaguchi, S. Hiroshima, T. Kodama, T. Kobayashi, T. A. Fukami, N. Oikawa, T.
691 Tsukuda, N. Ishii, Y. Aoki, CH5424802, a selective ALK inhibitor capable of blocking the resistant
692 gatekeeper mutant. *Cancer Cell* **19**, 679-690 (2011).
693 25. M. Tufail, C. Wu, SRPKs: a promising therapeutic target in cancer. *Clin Exp Med*, (2023).
694 26. I. P. Nikas, S. C. Themistocleous, S. A. Paschou, K. I. Tsamis, H. S. Ryu, Serine-Arginine Protein Kinase 1
695 (SRPK1) as a Prognostic Factor and Potential Therapeutic Target in Cancer: Current Evidence and Future
696 Perspectives. *Cells* **9**, (2019).
697 27. Z. Pogacar, K. Groot, F. Jochems, M. Dos Santos Dias, A. Mulero-Sanchez, B. Morris, M. Roosen, L.
698 Wardak, G. De Conti, A. Velds, C. Lieftink, B. Thijssen, R. L. Beijersbergen, R. Bernards, R. Leite de
699 Oliveira, Genetic and compound screens uncover factors modulating cancer cell response to indisulam. *Life*
700 *Sci Alliance* **5**, (2022).
701 28. J. Batson, H. D. Toop, C. Redondo, R. Babaei-Jadidi, A. Chaikuad, S. F. Wearmouth, B. Gibbons, C.
702 Allen, C. Tallant, J. Zhang, C. Du, J. C. Hancox, T. Hawtrey, J. Da Rocha, R. Griffith, S. Knapp, D. O.
703 Bates, J. C. Morris, Development of Potent, Selective SRPK1 Inhibitors as Potential Topical Therapeutics
704 for Neovascular Eye Disease. *ACS Chem Biol* **12**, 825-832 (2017).
705 29. E. M. Amin, S. Oltean, J. Hua, M. V. R. Gammons, M. Hamdollah-Zadeh, G. I. Welsh, M. K. Cheung, L.
706 Ni, S. Kase, E. S. Renne, K. E. Symonds, D. G. Nowak, B. Royer-Pokora, M. A. Saleem, M. Hagiwara, V.
707 A. Schumacher, S. J. Harper, D. R. Hinton, D. O. Bates, M. R. Ladomery, WT1 Mutants Reveal SRPK1 to
708 Be a Downstream Angiogenesis Target by Altering VEGF Splicing. *Cancer Cell* **20**, 768-780 (2011).

709 30. S. Burma, B. P. Chen, M. Murphy, A. Kurimasa, D. J. Chen, ATM phosphorylates histone H2AX in
710 response to DNA double-strand breaks. *J Biol Chem* **276**, 42462-42467 (2001).
711 31. J. M. Santos-Pereira, A. Aguilera, R loops: new modulators of genome dynamics and function. *Nat Rev*
712 *Genet* **16**, 583-597 (2015).
713 32. S. Hamperl, K. A. Cimprich, Conflict Resolution in the Genome: How Transcription and Replication Make
714 It Work. *Cell* **167**, 1455-1467 (2016).
715 33. S. C. Sridhara, S. Carvalho, A. R. Grosso, L. M. Gallego-Paez, M. Carmo-Fonseca, S. F. de Almeida,
716 Transcription Dynamics Prevent RNA-Mediated Genomic Instability through SRPK2-Dependent DDX23
717 Phosphorylation. *Cell Rep* **18**, 334-343 (2017).
718 34. E. Hatchi, K. Skourti-Stathaki, S. Ventz, L. Pinello, A. Yen, K. Kamieniarz-Gdula, S. Dimitrov, S.
719 Pathania, K. M. McKinney, M. L. Eaton, M. Kellis, S. J. Hill, G. Parmigiani, N. J. Proudfoot, D. M.
720 Livingston, BRCA1 recruitment to transcriptional pause sites is required for R-loop-driven DNA damage
721 repair. *Mol Cell* **57**, 636-647 (2015).
722 35. Y. Okamoto, M. Abe, A. Itaya, J. Tomida, M. Ishiai, A. Takaori-Kondo, M. Taoka, T. Isobe, M. Takata,
723 FANCD2 protects genome stability by recruiting RNA processing enzymes to resolve R-loops during mild
724 replication stress. *FEBS J* **286**, 139-150 (2019).
725 36. C. Mukherjee, V. Tripathi, E. M. Manolika, A. M. Heijink, G. Ricci, S. Merzouk, H. R. de Boer, J.
726 Demmers, M. van Vugt, A. Ray Chaudhuri, RIF1 promotes replication fork protection and efficient restart
727 to maintain genome stability. *Nat Commun* **10**, 3287 (2019).
728 37. D. D. Phillips, D. N. Garboczi, K. Singh, Z. Hu, S. H. Leppla, C. E. Leysath, The sub-nanomolar binding of
729 DNA-RNA hybrids by the single-chain Fv fragment of antibody S9.6. *J Mol Recognit* **26**, 376-381 (2013).
730 38. A. Promonet, I. Padioleau, Y. Liu, L. Sanz, A. Biernacka, A. L. Schmitz, M. Skrzypczak, A. Sarrazin, C.
731 Mettling, M. Rowicka, K. Ginalski, F. Chedin, C. L. Chen, Y. L. Lin, P. Pasero, Topoisomerase 1 prevents
732 replication stress at R-loop-enriched transcription termination sites. *Nat Commun* **11**, 3940 (2020).
733 39. K. C. Goldsmith, J. R. Park, K. Kayser, J. Malvar, Y. Y. Chi, S. G. Groshen, J. G. Villablanca, K. Krytska,
734 L. M. Lai, P. T. Acharya, F. Goodarzian, B. Pawel, H. Shimada, S. Ghazarian, L. States, L. Marshall, L.
735 Chesler, M. Granger, A. V. Desai, R. Mody, D. A. Morgenstern, S. Shusterman, M. E. Macy, N. Pinto, G.
736 Schleiermacher, K. Vo, H. C. Thurm, J. Chen, M. Liyanage, G. Peltz, K. K. Matthay, E. R. Berko, J. M.

737 Maris, A. Marachelian, Y. P. Mosse, Lorlatinib with or without chemotherapy in ALK-driven
738 refractory/relapsed neuroblastoma: phase 1 trial results. *Nat Med* **29**, 1092-1102 (2023).
739 40. Y. Suk, S. K. Singh, Safety and efficacy of lorlatinib against ALK-driven refractory or relapsed
740 neuroblastoma. *Cell Rep Med* **4**, 101071 (2023).
741 41. S. Peters, D. R. Camidge, A. T. Shaw, S. Gadgeel, J. S. Ahn, D. W. Kim, S. I. Ou, M. Perol, R.
742 Dziadziuszko, R. Rosell, A. Zeaiter, E. Mitry, S. Golding, B. Balas, J. Noe, P. N. Morcos, T. Mok, A. T.
743 Investigators, Alectinib versus Crizotinib in Untreated ALK-Positive Non-Small-Cell Lung Cancer. *N Engl*
744 *J Med* **377**, 829-838 (2017).
745 42. B. J. Solomon, G. Liu, E. Felip, T. S. K. Mok, R. A. Soo, J. Mazieres, A. T. Shaw, F. de Marinis, Y. Goto,
746 Y. L. Wu, D. W. Kim, J. F. Martini, R. Messina, J. Paolini, A. Polli, D. Thomaidou, F. Toffalorio, T. M.
747 Bauer, Lorlatinib Versus Crizotinib in Patients With Advanced ALK-Positive Non-Small Cell Lung
748 Cancer: 5-Year Outcomes From the Phase III CROWN Study. *J Clin Oncol* **42**, 3400-3409 (2024).
749 43. S. Singh, W. Quarni, M. Goralski, S. B. Wan, H. J. Jin, L. A. Van de Velde, J. Fang, Q. Wu, A. Abu-Zaid,
750 T. T. Wang, R. Singh, D. Craft, Y. P. Fan, T. Confer, M. Johnson, W. J. Akers, R. N. Wang, P. J. Murray,
751 P. G. Thomas, D. Nijhawan, A. M. Davidoff, J. Yang, Targeting the spliceosome through RBM39
752 degradation results in exceptional responses in high-risk neuroblastoma models. *Science Advances* **7**,
753 (2021).
754 44. S. Kohsaka, S. Yagishita, Y. Shirai, Y. Matsuno, T. Ueno, S. Kojima, H. Ikeuchi, M. Ikegami, R. Kitada,
755 K. I. Yoshioka, K. Toshimitsu, K. Tabata, A. Yokoi, T. Doi, N. Yamamoto, T. Owa, A. Hamada, H. Mano,
756 A molecular glue RBM39-degrader induces synthetic lethality in cancer cells with homologous
757 recombination repair deficiency. *NPJ Precis Oncol* **8**, 117 (2024).
758 45. E. R. Tucker, I. Jimenez, L. Chen, A. Bellini, C. Gorrini, E. Calton, Q. Gao, H. Che, E. Poon, Y. Jamin, B.
759 Martins Da Costa, K. Barker, S. Shrestha, J. C. Hutchinson, S. Dhariwal, A. Goodman, E. Del Nery, P.
760 Gestraud, J. Bhalshankar, Y. Iddir, E. Saberi-Ansari, A. Saint-Charles, B. Geoerger, M. E. Marques Da
761 Costa, C. Pierre-Eugene, I. Janoueix-Lerosey, D. Decaudin, F. Nemati, A. M. Carcaboso, D. Surdez, O.
762 Delattre, S. L. George, L. Chesler, D. A. Tweddle, G. Schleiermacher, Combination Therapies Targeting
763 ALK-aberrant Neuroblastoma in Preclinical Models. *Clin Cancer Res* **29**, 1317-1331 (2023).

764 46. B. Y. Tam, K. Chiu, H. Chung, C. Bossard, J. D. Nguyen, E. Creger, B. W. Eastman, C. C. Mak, M.
765 Ibanez, A. Ghias, J. Cahiwat, L. Do, S. Cho, J. Nguyen, V. Deshmukh, J. Stewart, C. W. Chen, C. Barroga,
766 L. Dellamary, S. K. Kc, T. J. Phalen, J. Hood, S. Cha, Y. Yazici, The CLK inhibitor SM08502 induces anti-
767 tumor activity and reduces Wnt pathway gene expression in gastrointestinal cancer models. *Cancer Lett*
768 **473**, 186-197 (2020).
769 47. M. Sakuma, K. Iida, M. Hagiwara, Deciphering targeting rules of splicing modulator compounds: case of
770 TG003. *Bmc Mol Biol* **16**, (2015).
771 48. M. Buljan, R. Ciuffa, A. van Drogen, A. Vichalkovski, M. Mehnert, G. Rosenberger, S. Lee, M. Varjosalo,
772 L. E. Pernas, V. Spegg, B. Snijder, R. Aebersold, M. Gstaiger, Kinase Interaction Network Expands
773 Functional and Disease Roles of Human Kinases. *Mol Cell* **79**, 504-520 e509 (2020).
774 49. E. R. Tucker, J. R. Tall, L. S. Danielson, S. Gowan, Y. Jamin, S. P. Robinson, U. Banerji, L. Chesler,
775 Immunoassays for the quantification of ALK and phosphorylated ALK support the evaluation of on-target
776 ALK inhibitors in neuroblastoma. *Mol Oncol* **11**, 996-1006 (2017).
777
778

Acknowledgments: We are very grateful to the technicians from the Institute of Cancer Research BSU animal center, Barbara Martins da Costa and Kevin Greenslade for supporting animal work. We thank Prof. Matthew J Fuchter from Imperial College London and Dr Lizzie Tucker from Institute of Cancer Research for providing helpful comments.

Funding: Imperial College London and China Scholarship Council joint PhD studentship 202208310101 (YM), 201808060050 (YX). AstraZeneca/NIHR Imperial BRC Imperial College Research Fellowship (AN). Cancer Research UK Fellowship RCCCDF-Nov23/100003 (AN). Cancer Research UK Discovery Programme Grant (A28278) (EP, BMC, LC); HEFCE/RAE (LC). Ovarian Cancer Action (CW, AN). Cancer Research UK convergence Science Centre PhD studentships SEBCATP-2024/100009 (NZ), CANCTA-2022\100007 (SQ).

Author contributions:

Conceptualization: YM, AN, HCK

Methodology: YM, EP, YX, SQ, AN

Investigation: YM, EP, BMC, YX, CJ, SQ, NZ, LC, HCK, AN

Visualization: YM, YX, CJ, SQ, AN

Funding acquisition: LC, HCK, AN

Project administration: HCK, AN

Supervision: AN, HCK, LC,

Writing – original draft: YX, LC, HCK, AN

Writing – review & editing: all authors contributed to the review and editing of the paper.

Competing interests: Authors declare that they have no competing interests.

Data and materials availability: All data supporting the conclusions of this paper are available within the main text and/or Supplementary Materials.